DRAFT VERSION AUGUST 4, 2016
Preprint typeset using LaTeX style emulateapj v. 5/2/11

WHIMPER OF A BANG: DOCUMENTING THE FINAL DAYS OF THE NEARBY TYPE IA SUPERNOVA 2011FE

B. J. SHAPPEE[1,2], K. Z. STANEK[3,4], C. S. KOCHANEK[3,4], AND P. M. GARNAVICH[5]

Draft version August 4, 2016

ABSTRACT

Using the Hubble Space Telescope (*HST*) and the Large Binocular Telescope, we followed the evolution of the Type Ia supernova (SN Ia) 2011fe for an unprecedented 1622 days past *B*-band maximum light and over a factor of 5 million in flux. At 1622 days, the 4000 – 17000 Å quasi-bolometric luminosity is just $(710 \pm 30)\,L_{\odot}$. By measuring the late-time quasi-bolometric light curve we present the first confident detection of ^{57}Co decay in a SN Ia light curve and estimate a mass ratio of $\log(^{57}\mathrm{Co}/^{56}\mathrm{Co}) = -1.62^{+0.08}_{-0.09}$. We do not have a clean detection of ^{55}Fe, but find a limit of $^{55}\mathrm{Fe}/^{57}\mathrm{Co} < 0.3$ with 90% confidence. These abundance ratios provide unique constraints on the progenitor system because the central density of the exploding white dwarf(s) dictates these nucleosynthetic yields. The observed ratios strongly prefer the lower central densities of double-degenerate models ($^{55}\mathrm{Fe}/^{57}\mathrm{Co} = 0.27$) over the higher central densities of near Chandrasekhar-mass single-degenerate models ($^{55}\mathrm{Fe}/^{57}\mathrm{Co} = 0.68$). We will continue to observe SN 2011fe for another ~ 900 days with *HST* and possibly beyond.

Subject headings: supernovae: Type Ia — supernovae: individual (SN 2011fe) — white dwarfs

1. INTRODUCTION

Although it is generally accepted that SNe Ia are produced in close binary systems where the constituents interact, there are still two competing classes of models. The double-degenerate (DD) model consists of a binary system with two white dwarfs (WDs) that merge either due to the removal of energy and angular momentum from the system by gravitational radiation (Tutukov & Yungelson 1979; Iben & Tutukov 1984; Webbink 1984) or due to the perturbations of a third (e.g., Thompson 2011; Katz & Dong 2012; Shappee & Thompson 2013; Antognini et al. 2014) or fourth (Pejcha et al. 2013) body. The single-degenerate (SD) model consists of a WD primary and a non-degenerate secondary. Most current work on the SD model focuses on systems in which the primary accretes matter from the secondary until the primary becomes unstable to run-away nuclear burning.

The search for observational signatures capable of distinguishing between these two models has been difficult. Most DD models effectively have no direct signatures. The SD model is thought to have observable consequences and some classes of SD models have been observationally ruled out as the dominant channel (e.g., Leonard 2007; Bianco et al. 2011; Chomiuk et al. 2016; Maguire et al. 2016), but there are a number of systems which are considered to be candidates (e.g. U Sco and V445 Pup; Li et al. 2011) and there might be multiple channels for producing normal SNe Ia (e.g., Maguire et al. 2013; Yamaguchi et al. 2015). Current explosion simulations of both SD (e.g. Kasen et al. 2009) and DD (e.g. Pakmor et al. 2012) progenitors can match the observable signatures of SNe Ia around *B*-band maximum light ($t_{B\mathrm{max}}$). Thus, the nature of the progenitor systems of SNe Ia remains a largely unsolved problem in modern astronomy.

The very-late-time light curves of SNe Ia are a powerful test of these two scenarios. The near-Chandrasekhar-mass WDs of the SD scenario have much higher central densities than the lower-mass WDs of the DD scenario, which leads to significant differences in the nucleosynthetic yields (Röpke et al. 2012). Most important for this study, the higher-density near-Chandrasekhar-mass WDs produce significantly more ^{55}Co and ^{55}Fe. For example, Röpke et al. (2012) found in their 3D simulations that the SD (DD) model produced $0.019\mathrm{M}_{\odot}$ ($0.015\mathrm{M}_{\odot}$) of ^{57}Ni and ^{57}Co combined, and $0.013\mathrm{M}_{\odot}$ ($0.004\mathrm{M}_{\odot}$) of ^{55}Co and ^{55}Fe combined, respectively. At very late times (> 1050 days after $t_{B\mathrm{max}}$), ^{57}Co and ^{55}Fe become the dominant power source for SNe Ia light curves through the following decay chains (Seitenzahl et al. 2009),

$$^{56}\mathrm{Ni} \xrightarrow{t_{1/2}=6.08d} {}^{56}\mathrm{Co} \xrightarrow{t_{1/2}=77.2d} {}^{56}\mathrm{Fe} \quad (1)$$

$$^{57}\mathrm{Ni} \xrightarrow{t_{1/2}=35.60h} {}^{57}\mathrm{Co} \xrightarrow{t_{1/2}=271.79d} {}^{57}\mathrm{Fe} \quad (2)$$

$$^{55}\mathrm{Co} \xrightarrow{t_{1/2}=17.53h} {}^{55}\mathrm{Fe} \xrightarrow{t_{1/2}=999.67d} {}^{55}\mathrm{Mn}. \quad (3)$$

Because of the abundance variations between the two scenarios, the predicted bolometric luminosity > 1600 days after $t_{B\mathrm{max}}$ differs by $> 50\%$ between the SD and DD models (Röpke et al. 2012). Thus, very-late-time bolometric observations of SNe Ia should be a strong diagnostic of these nuclear yields, and discriminate between progenitor models.

However, observing SNe Ia at very-late times has proven extremely difficult. The latest observations of a SNe Ia before this work were long-pass (*F*350*LP*) observations of SN 2012cg taken by the Hubble Space telescope (*HST*) 1055 days after $t_{B\mathrm{max}}$. Through these observations, Graur et al. (2016) may have been the first to observe the decay of ^{57}Co powering a SN Ia light curve, but their observations were also consistent with a light echo. SN 2012cg was not observable at late enough times to constrain the presence of ^{55}Fe.

The recent SN Ia 2011fe is our best opportunity to observe

bshappee@obs.carnegiescience.edu
[1] Carnegie Observatories, 813 Santa Barbara Street, Pasadena, CA 91101, USA
[2] Hubble, Carnegie-Princeton Fellow
[3] Department of Astronomy, The Ohio State University, 140 West 18th Avenue, Columbus, OH 43210, USA
[4] Center for Cosmology and AstroParticle Physics (CCAPP), The Ohio State University, 191 W. Woodruff Ave., Columbus, OH 43210, USA
[5] Department of Physics, University of Notre Dame, Notre Dame, IN 46556, USA

a SN Ia at extremely late times. SN 2011fe was discovered less than one day after the explosion by the Palomar Transient Factory (Law et al. 2009) in a sparse region of the outer disk of the well-studied, face-on spiral M101. SN 2011fe became the brightest SN Ia in almost 40 years and exploded a mere 6.4 Mpc away (Shappee & Stanek 2011). Its early discovery allowed extensive multi-wavelength follow-up observations to be quickly carried out and these studies have shown that SN 2011fe was a "plain vanilla" SN Ia (Wheeler 2012), remarkable only in its proximity. Li et al. (2011) and Graur et al. (2014) used pre-explosion *HST* images to constrain the progenitor system of SN 2011fe. Li et al. (2011) did not detect any counterpart at the location of the SN and placed 2σ upper limits of F435W < 27.87, F555W < 27.49, and F814W < 26.81 at its position. Patat et al. (2013) obtained high-resolution spectra of SN 2011fe and found that it is only slightly reddened and appears to be surrounded by a "clean" environment with a total reddening from both the Milky Way and M101 of $E(B-V) \lesssim 0.05$ mag. Dust is expected to form in the ejecta of SNe Ia $\sim 100-300$ days after $t_{B\max}$ (Nozawa et al. 2011). However, there is no evidence for dust formation during the first 3 years (Kerzendorf et al. 2014) and the optical depth would drop as t^{-2}, so dust extinction is unimportant for late-time observations of SN 2011fe. Additionally, very-late-time (~ 1000 days after $t_{B\max}$) spectroscopic observations showed no evidence of any light echoes (Graham et al. 2015a, Taubenberger et al. 2015, Shappee et al. in prep.). These factors make SN 2011fe an exceptional opportunity to put the strongest constraints on the progenitor system of any SN Ia. While SN 2014J (Fossey et al. 2014) is still closer, it is not a good candidate for late-time studies because it is highly obscured (e.g., Brown et al. 2015), located in a crowded, dense environment, and is already showing evidence of light echoes (Crotts 2015).

The data available for SN 2011fe are unparalleled, with multi-wavelength studies in the radio (Horesh et al. 2012; Chomiuk et al. 2012), the far-IR with Herschel (Johansson et al. 2013), the mid-IR with Spitzer (McClelland et al. 2013), the IR (Matheson et al. 2012), the optical (Nugent et al. 2011; Smith et al. 2011; Richmond & Smith 2012; Munari et al. 2013; Shappee et al. 2013b; Patat et al. 2013; Pereira et al. 2013; Tsvetkov et al. 2013; Kerzendorf et al. 2014; Graham et al. 2015b,a; Lundqvist et al. 2015; Shappee et al. 2015a; Zhang et al. 2016; Friesen et al. 2016), the UV with SWIFT (Nugent et al. 2011; Brown et al. 2012) and *HST* (Foley & Kirshner 2013; Mazzali et al. 2014; Friesen et al. 2016), X-rays with SWIFT (Horesh et al. 2012; Margutti et al. 2012) and Chandra (Margutti et al. 2012), and gamma rays (Isern et al. 2013). By looking for observational signatures from the companion, many of these studies have already placed constraints on SNe Ia progenitor models. For example, Brown et al. (2012) and Shappee et al. (2013b) have claimed to rule out the canonical SD channel where the companion is a normal red giant or main sequence star. However, Justham (2011) and Di Stefano & Kilic (2012) have suggested a way to avoid these limits by using rotational support of the WD to delay the explosion long enough for the companion to evolve into a detached, smaller, and fainter star. Alternatively, Wheeler (2012) suggests that the companion could be a less massive M dwarf with a smaller radius than previously considered. These variations on the SD model highlight the need to have a direct probe into the properties of the exploding WD(s) instead of just relying on possible interactions with a companion for observational signatures.

TABLE 1
PHOTOMETRIC OBSERVATIONS

JD (–2,450,000)	Band	Mag. | Bol. Flux $\cdots$ | [10^{36} ergs/s]	Telescope
6008.836	$U_{\rm spec}$	16.31(0.01)	LBT/LBC
6302.987	B	20.14(0.02)	LBT/LBC
6303.001	V	20.11(0.02)	LBT/LBC
6302.993	R	20.68(0.02)	LBT/LBC
6050.000	J	17.18(0.10)	LBT/LUCI
6939.664	$F438W$	24.96(0.08)	HST/WFC3/UVIS
6939.653	$F555W$	24.48(0.02)	HST/WFC3/UVIS
6939.667	$F600LP$	24.84(0.02)	HST/WFC3/UVIS
6939.664	$F110W$	24.30(0.04)	HST/WFC3/IR
6939.789	$F160W$	22.37(0.02)	HST/WFC3/IR
6939.664	bol	13.74(0.19)	HST/WFC3

NOTE. — Photometric and bolometric light curves. Photometry is calibrated in the Vega magnitude system and the bolometric light curve is in units of 10^{36} ergs/s. *Only the first observation in each band is shown here to demonstrate its form and content. The table is included in its entirety as an ancillary file.*

In Section 2, we describe our observations. In Section 3, we constrain the pre-explosion variability at the site of SN 2011fe. In Section 4, we construct a late-time quasi-bolometric light curve of SN 2011fe and use it to place constraints on the progenitor system. In Section 5, we discuss possible sources of contamination in our quasi-bolometric light curve. Finally, we discuss our results in Section 6. Throughout this paper we assume SN 2011fe is at a distance of 6.4 ± 0.5 Mpc (Shappee & Stanek 2011), has a Milky Way reddening of $E(B-V) = 0.009$ mag (Schlegel et al. 1998) with a ratio of total-to-selective absorption of $R_V = 3.1$ (Cardelli et al. 1989), and had no host galaxy extinction (e.g., Patat et al. 2013).

2. OBSERVATIONS

We analyzed pre- and post-explosion images of SN 2011fe from the Large Binocular Camera (LBC; Giallongo et al. 2008) and the NIR spectrograph LUCI (Seifert et al. 2003) on the Large Binocular Telescope (*LBT*) and the Wide Field Camera 3 (WFC3) and the Advanced Camera for Surveys (ACS) on *HST*. Our last epoch of WFC3 imaging and archival, pre-explosion ACS imaging at the location of SN 2011fe are shown in Figure 1. The SN is easily seen even in our last epoch. In Figure 2 we show the throughput of the optical filters used in this work along with a spectrum of SN 2011fe acquired 1016 days after $t_{B\max}$ using MODS on the *LBT* (Taubenberger et al. 2015). The photometry is presented in Table 1 and shown in Figures 3 and 4.

We obtained 28 epochs of *LBT*/LBC $U_{\rm spec}-$, $B-$, $V-$, and $R-$band imaging of M101 between March 2008 and February 2016 as part of a program searching for failed SNe (Kochanek et al. 2008; Gerke et al. 2011, 2015). The pre-explosion images allowed us to construct deep reference images without having to wait for SN 2011fe to completely fade. The data were analyzed with the `ISIS` image-subtraction package (Alard & Lupton 1998; Alard 2000). We then performed aperture photometry on the subtracted images using the IRAF `apphot` package and calibrated the magnitudes using the SDSS Data Release 10 (DR10; Ahn et al. 2014) photometry of nearby fields stars transformed into Bessel filters using Lupton (2005)[6]. We note that the Zhang et al. (2016) U-band

[6] http://www.sdss.org/dr12/algorithms/

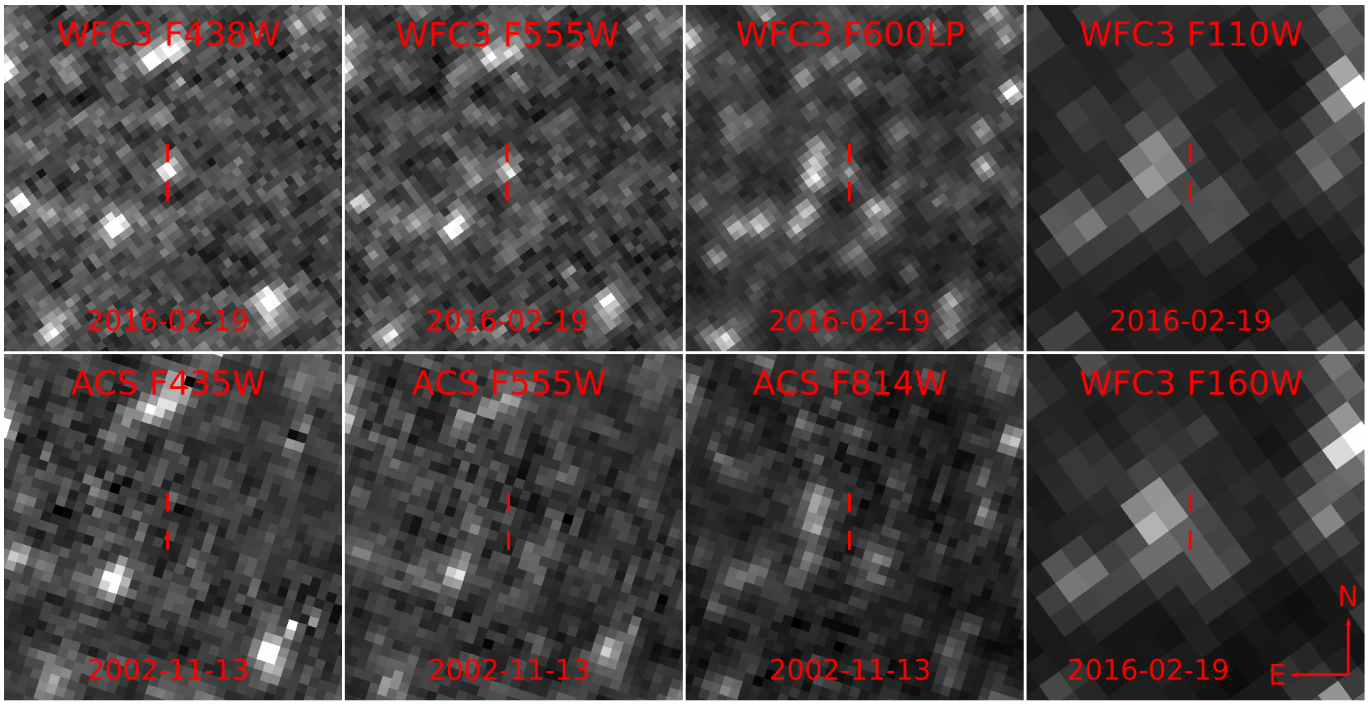

FIG. 1.— Late-time (1622 days after $t_{B\mathrm{max}}$) and archival pre-explosion (GO9490; PI: K. Kuntz) *HST* images of the location of SN 2011fe. The tick marks are 0.″1 long and indicate our measured position for SN 2011fe (RA = $14^{\mathrm{h}}03^{\mathrm{m}}05^{\mathrm{s}}.740$ Dec = +54° 16′ 25.″24 J2000; astrometric coordinates referenced to the WCS solution of icoy01080_drz.fits).

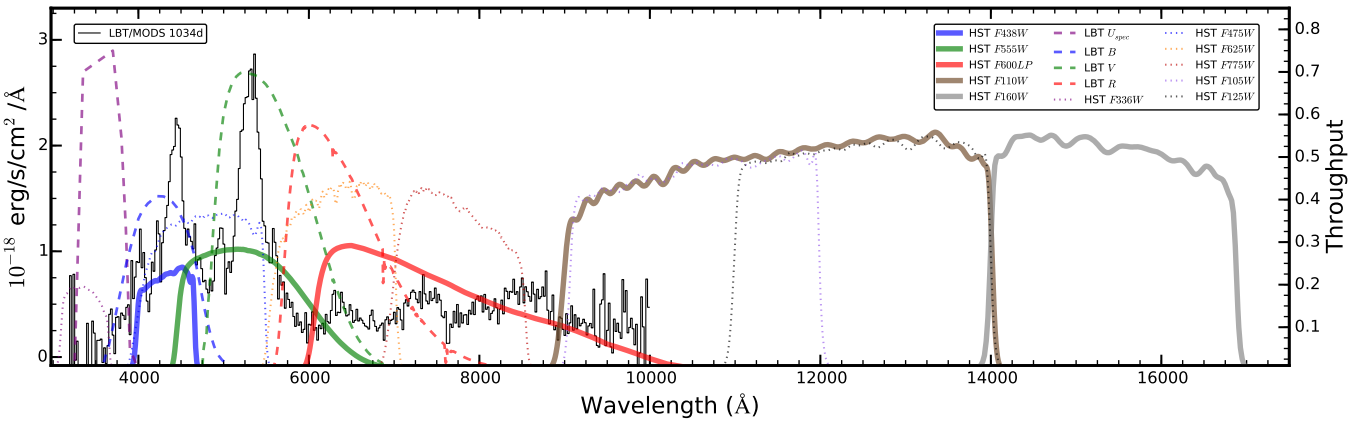

FIG. 2.— Throughput functions for the filters used in this work as compared to the Taubenberger et al. (2015) MODS/*LBT* spectrum of SN 2011fe taken 1016 days after $t_{B\mathrm{max}}$.

observations disagree with our first two U_{spec} epochs and the Tsvetkov et al. (2013) observations.

We also obtained 3 epochs of *LBT*/LUCI J–band imaging of SN 2011fe between May 2012 and February 2013. The photometry was obtained from J-band acquisition images for LUCI spectroscopy (Mazzali et al. 2015). Dithered pairs of J-band images were subtracted and aperture photometry was applied to the supernova and to three 2MASS catalog stars in the field for calibration.

We also obtained 4 epochs of *HST* data using the WFC3 UVIS and IR cameras (GO-13737 and 14166) starting in October 2014. We used the WFC3/UVIS $F438W$ (B), $F555W$ (V), $F600LP$ ($R+I$), $F110W$ ($Y+J$), and $F160W$ (H) filters because the very-late-time spectra of SNe Ia predominantly consists of line emission over a very broad range of wavelengths redward of the UV (see Figure 2). This filter combination was selected for several reasons: 1) The filters cover 4000 to 17000Å with no gaps and relatively uniform throughput. Ground-based spectroscopy and photometry showed there is little flux blueward of 4000 Å so we did not include the F336W (U) or UV filters. 2) A single (or two) long pass filter(s) would not be sufficient because the shape of the SN spectral energy distribution (SED) is known to be changing with the ionization state (McClelland et al. 2013; Graham et al. 2015a; Taubenberger et al. 2015, Shappee et al. in prep.). Computing the bolometric luminosity with a single F350LP observation would lead to large systematic uncertainties because we could mistake a change in ionization state for a change in the bolometric luminosity or interpret a light echo as a flattening of the bolometric light curve. 3) Finally, this optical filter combination evenly partitions the emission seen in the 1016-day spectrum obtained by Taubenberger et al. (2015) across the filters.

sdssUBVRITransform/#Lupton2005

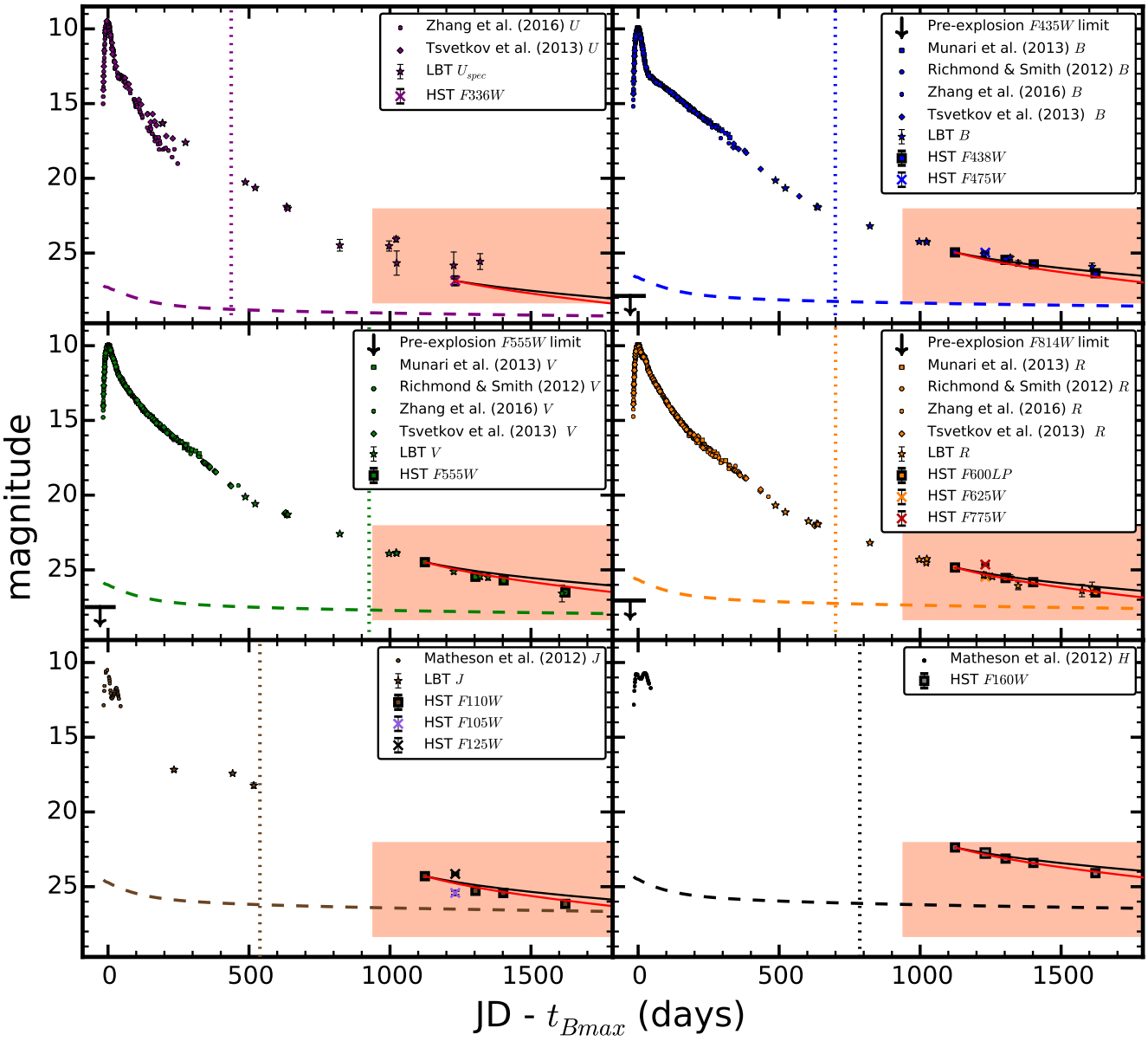

FIG. 3.— *HST* (filled squares and crosses), *LBT* (filled stars), and published (indicated in legends) light curves of SN 2011fe. The uncertainties are shown for the *LBT* and *HST* observations but can be smaller than the points. The vertical dotted lines show the previously latest SN Ia observations in each filter excluding examples of light echoes (Stritzinger & Sollerman 2007; Leloudas et al. 2009; Cappellaro et al. 1997). The horizontal dashed lines show the expected brightness of a shock-heated 1 $M_\odot$ MS companion (Shappee et al. 2013a) for each filter. The solid black and solid red lines show the Röpke et al. (2012) SD and DD models, respectively, scaled to fit the first *HST* observation. Black arrows just below t = 0 days indicate the Li et al. (2011) 2-sigma pre-explosion upper limits. The orange highlighted region is shown in Figure 4.

We measured the instrumental Vega Magnitudes using the WFC3 module of the DOLPHOT stellar photometry package[7] for our WFC3 observations. For each of the UVIS images, we first corrected for charge-transfer efficiency (CTE) at the pixel level using the WFC3/UVIS CTE tool [8]. The NIR was not as simple as the optical because SN 2011fe is blended with nearby, very-red stars in the NIR (see Figure 1). First, we determined the precise position of SN 2011fe and the nearby stars in the $F110W$ and $F160W$ images by using the higher-resolution $F600LP$ images. With the recommended parameters, DOLPHOT correctly found the nearby stars and SN 2011fe for the 1124– and 1403– day epochs. However, for the 1302– and 1622–day epochs we had to adjust the source thresholds and maximum iterations for DOLPHOT to correctly identify these sources. Finally, we verified the flux differences between epochs by subtracting epochs with ISIS. SN 2011fe is clearly visible in these subtractions and the flux differences are consistent with our reported DOLPHOT photometry.

However, Williams et al. (2014) found that the photon statistics errors reported by DOLPHOT for the Panchromatic Hubble Andromeda Treasury survey tended to underestimate uncertainties by a factor of a few. We corrected the uncertainties of our HST photometry separately for the optical and

[7] http://americano.dolphinsim.com/dolphot/
[8] http://www.stsci.edu/hst/wfc3/tools/cte_tools

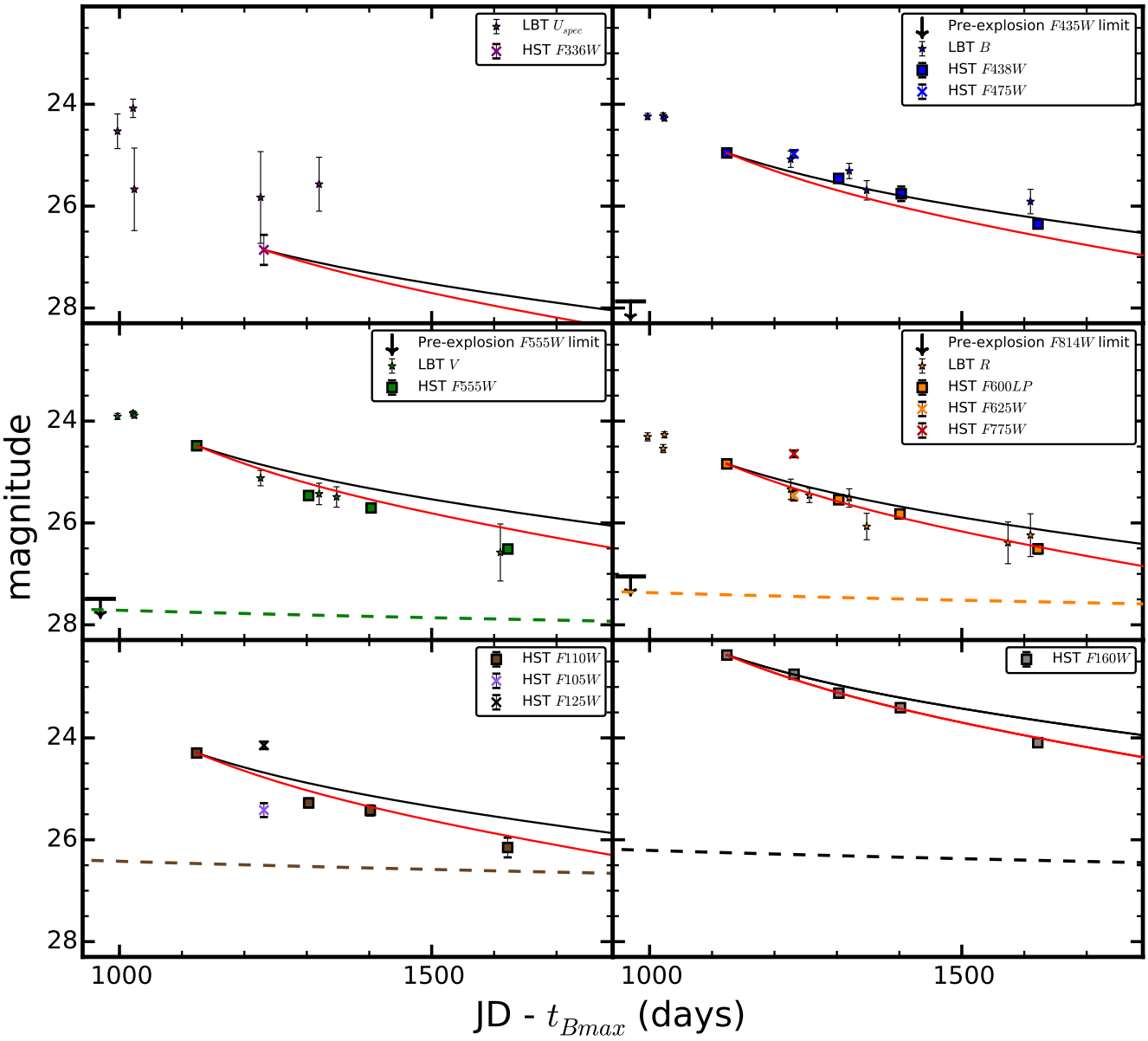

FIG. 4.— *HST* (filled squares and crosses) and *LBT* (filled stars) late-time light curves of SN 2011fe. The uncertainties are shown but are smaller than the points in some cases. The horizontal dashed lines show the expected brightness of a shock-heated 1 $M_\odot$ MS companion (Shappee et al. 2013a) for each filter. The solid black and solid red lines show the Röpke et al. (2012) SD and DD models, respectively, scaled to fit the first *HST* observation. Black arrows just below t = 1000 days indicate the Li et al. (2011) 2-sigma pre-explosion upper limits.

NIR by analyzing the DOLPHOT light curves for point sources within 18.″0 of the SN. We required that sources were detected in all four epochs within the magnitude range observed for SN 2011fe in our HST data. We then removed high-amplitude variable stars, defined by those with Stetson $F555W/F600LP$ or $F110W/F160W$ variability indices $I > 10$ (Stetson 1996), leaving 149 stars in the optical and 262 stars in the NIR to calibrate our errors. For each star we determined the ratio of the deviation from the star's mean magnitude to the error reported by DOLPHOT in each epoch. We then scaled the DOLPHOT errors of SN 2011fe by the median of these ratios for each filter and epoch separately. All uncertainties were scaled by less than a factor of 2, except for the $F438W$ filter's 1403−day epoch which was scaled by a factor of 4.4.

Finally, for completeness, we also present archival *HST* WFC3/UVIS, ACS, and WFC3/IR photometry in the F336W (U), F475W (g), F625W (r), F775W (i), F105W (Y), F125W (J) and F160W (H) filters acquired during January 2015 (GO-13824; PI W. Kerzendorf). We treat the WFC3 data as described above and we perform photometry on the ACS data using the ACS module of the DOLPHOT stellar photometry package. We did not scale this photometry's errors because only a single epoch of observation is available. This photometry is consistent with ours as seen in Figure 4.

3. PRE-EXPLOSION *LBT* VARIABILITY CONSTRAINTS

We have 7, 9, 9, and 8 epochs of *LBT*/LBC data obtained between March 2008 and December 2010 observed in U, B, V, and R, respectively. Gerke et al. (2014) previously used a similar dataset of M82 to set a limit on the pre-explosion

R-band variability at the location for SN 2014J of $\Delta|\nu L_\nu| < 3000\ L_\odot$ (3σ) over the 6 years prior to the SN. We observe no pre-explosion variability at the location of SN 2011fe and we place 3-sigma limits on the pre-SN variability in U, B, V, and R of 6.1×10^{36}, 2.5×10^{36}, 6.1×10^{36}, and 2×10^{36} erg s^{-1} or ~ 2000, ~ 1000, ~ 2000, and $\sim 1000\ L_\odot$, respectively. Interpolating linearly between the filters and extrapolating using a constant f_λ, we find a variability limit of 1.2×10^{37} erg s^{-1} or $\sim 3000\ L_\odot$ over the wavelength range from 3000 – 8000 Å .

4. QUASI-BOLOMETRIC LIGHT CURVE AND PROGENITOR CONSTRAINTS

In this section we construct a quasi-bolometric light curve for SN 2011fe, place constraints on the progenitor assuming our quasi-bolometric light curve is representative of the true bolometric light curve, and compute the fraction of the bolometric luminosity emitted in our observed wavelengths.

4.1. *Quasi-Bolometric Light Curve*

The quasi-bolometric light curve for SN 2011fe was computed over the wavelength region that our photometric observations probe, from 4000 – 17000 Å. To reduce the systematic errors in the calculation, we did not assume the optical SED was a simple interpolation over the photometric bands, but instead used the Taubenberger et al. (2015) 1016-day MODS/*LBT* spectrum of SN 2011fe as a template and iteratively fit it to the observed photometry. For the NIR there exist no published late-time spectra. Instead we averaged f_λ from 9000 – 10000 Å in the 1016-day MODS/*LBT* spectrum and assumed a flat f_λ spectrum from 10000 – 17000 Å. We then performed synthetic photometry from this constructed spectrum for the $F438W$, $F555W$, $F600LP$, $F110W$, and $F160W$ bands. We computed the differences between the synthetic and observed photometry, linearly interpolated these differences at each filter's effective wavelength, and then warped the spectrum by this interpolation. We iterated this process until the synthetic and observed photometry matched to better than 0.001 mag in each filter. The warped SEDs for each epoch are shown in Figure 5. The errors on the quasi-bolometric light curve were computed through Monte Carlo re-sampling the input photometry and then recomputing the quasi-bolometric light curve. The quasi-bolometric light curve for SN 2011fe is shown in Figure 6 and presented in Table 1.

Finally, because SN 2011fe is crowded in the NIR, its photometry might be questionable and affect our analysis based on the quasi-bolometric light curve. To alleviate this concern, we also repeated the quasi-bolometric light curve calculation using only the optical data (4000 – 9500 Å) where SN 2011fe is well isolated and pre-explosion observations show no sources to limits fainter than SN 2011fe in our last epoch. We then duplicated the entire analysis that follows and obtained qualitatively similar results.

4.2. *Progenitor Constraints*

We constrain the progenitor models by assuming the quasi-bolometric light curve computed in Section 4 tracks the true bolometric decay of SN 2011fe. Milne et al. (2001) showed that this is likely a good assumption at earlier times, between ~ 50 and 600 days, where the V band scales with the bolometric luminosity. We fit the quasi-bolometric light curve using Bateman's equation for the radioactive-decay chains of ^{56}Ni, ^{57}Ni and ^{55}Co presented in Equations 1-3. We assume the decay energies presented in Table 1 of Seitenzahl et al. (2009); that the SN ejecta is transparent to γ-rays; that e^-, e^+, and X-rays instantaneously deposit their energy; and that deposited energy is immediately radiated. Section 3 of Graur et al. (2016) provides a discussion and justification of these assumptions.

First, we fit the Röpke et al. (2012) predicted abundances for ^{56}Ni, ^{57}Ni and ^{55}Co from their SD and DD models to the bolometric light curve. Because we cannot observe SN 2011fe at all wavelengths we are not able to make true calorimetric measurements of SN 2011fe and thus we cannot make absolute abundance measurements from our quasi-bolometric light curve. However, we are able to make relative abundance measurements by assuming the quasi-bolometric light curve is proportional to the true bolometric light curve. We found that the quasi-bolometric light curve of SN 2011fe strongly prefers the DD model ($\chi^2 = 16.8$ with $\nu = 3$ degrees of freedom) over the SD model ($\chi^2 = 196.4$ with $\nu = 3$). The majority of this χ^2 difference is due to the data preferring the lower ^{55}Fe/^{57}Co ratio predicted from nuclear burning at lower densities.

We used the `emcee` package (Foreman-Mackey et al. 2013), a Python-based implementation of the affine-invariant ensemble sampler for Markov chain Monte Carlo (MCMC), to fit the quasi-bolometric light curve with the ratios ^{57}Co/^{56}Ni and ^{55}Fe/^{57}Co as free parameters. We found log(^{57}Co/^{56}Ni) and log(^{55}Fe/^{57}Co) abundance ratios of $-1.62^{+0.08}_{-0.09}$ and $-1.0^{+0.3}_{-0.5}$, respectively. Our best fit had a $\chi^2 = 4.1$ with $\nu = 1$ for abundance ratios of ^{57}Co/^{56}Ni = 0.03 and ^{55}Fe/^{57}Co = 0.08. Finally, we fit the quasi-bolometric light curve excluding either ^{57}Co or ^{55}Fe, finding $\chi^2 = 73.2$ and $\chi^2 = 4.7$, respectively, for $\nu = 2$. In practice, the present light curve can be explained using only ^{56}Ni and ^{57}Co with an upper limit on the ^{55}Fe abundance ration of ^{55}Fe/^{57}Co < 0.3 at 90% confidence. This upper limit strongly favors the Röpke et al. (2012) DD model (^{55}Fe/^{57}Co = 0.27) over their SD model (^{55}Fe/^{57}Co = 0.68).

Using only the optical data to construct the bolometric light curve leads to similar results. In particular, the models require the presence of ^{57}Co but not ^{55}Fe. For the model with all the isotope masses allowed to vary we find log(^{57}Co/^{56}Ni) = $-1.59^{+0.09}_{-0.11}$ and ^{55}Fe/^{57}Co < 0.3 at 90% confidence. Our best fit had a $\chi^2 = 1.6$ with $\nu = 1$ for abundance ratios of ^{57}Co/^{56}Ni = 0.03 and ^{55}Fe/^{57}Co = 0.04. These ratios are consistent with the results including the NIR flux.

4.3. *Fraction of the Total Bolometric Luminosity emitted in the Optical/NIR*

Although we cannot determine the absolute abundance of ^{56}Ni, we can use previous estimates of $M_{^{56}\mathrm{Ni}}$ for SN 2011fe to determine the fraction of the decay energy, excluding γ-rays, which is encompassed by our quasi-bolometric light curve. There have been three previous studies which measured the total ^{56}Ni yield for SN 2011fe. Pereira et al. (2013) used an early-time UltraViolet Optical near-InfraRed (UVOIR) bolometric light curve and Arnett's rule (e.g., Stritzinger et al. 2006) and found $M_{^{56}\mathrm{Ni}} = 0.53 \pm 0.11\ M_\odot$. Childress et al. (2015) examined the evolution of the [Co III] λ5893 emission complex during the nebular phase and estimate $M_{^{56}\mathrm{Ni}} = 0.500 \pm 0.026_{\mathrm{stat}} \pm 0.069_{\mathrm{sys}}\ M_\odot$. Finally, Mazzali et al. (2015)

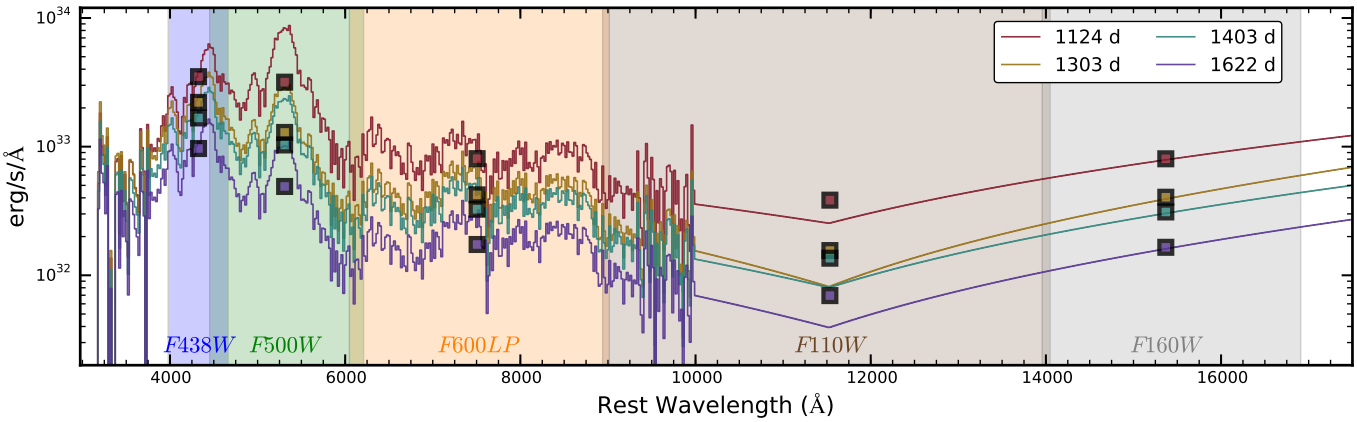

FIG. 5.— Late-time SED for SN 2011fe. Squares show our HST observations at their effective wavelengths. Solid lines show the fit SED as described in Section 4.1. Synthetic photometry of the SED are not expected to go through the *HST* photometry, but instead agree to better than 0.001 mag with the filter-averaged values in each filter. The color of symbols and lines distinguish between epochs. The shaded regions indicate where each filter's throughput is $> 10\%$.

used optical and near-infrared nebular spectra to estimate that $M_{^{56}\mathrm{Ni}} = 0.47 \pm 0.05$ M$_\odot$. The weighted mean of these measurements, assuming their random errors are independent, is $M_{^{56}\mathrm{Ni}} = 0.50 \pm 0.02$ M$_\odot$.

In our fit to the quasi-bolometric light curve with the abundances of ^{56}Ni, ^{57}Ni, and ^{55}Co as free parameters, we find that $M_{^{56}\mathrm{Ni}} = 0.30^{+0.03}_{-0.03}$ M$_\odot$ is needed to explain the observed flux. This implies that 0.60 ± 0.07 of the bolometric luminosity is being emitted from 4000 – 17000 Å independent of the primary uncertainty in the luminosity (the distance). This estimate is dominated by our first epoch where ^{56}Ni still dominates the emission. Combining the early-time measurement of $M_{^{56}\mathrm{Ni}}$ and our measured ^{57}Co/^{56}Ni we find $M_{^{57}\mathrm{Co}} = 0.012^{+0.002}_{-0.002}$ M$_\odot$ in tension with the Fransson & Jerkstrand (2015) estimate of ~ 0.02 M$_\odot$. Furthermore, finding that 0.60 ± 0.07 of the emission is in the optical/NIR is substantially higher than the $\sim 20\%$ predicted by Fransson & Jerkstrand (2015). Even if we just measure the optical emission (4000 – 9500 Å), it represents 0.40 ± 0.06 of the bolometric emission expected from $M_{^{56}\mathrm{Ni}} = 0.50 \pm 0.02$ M$_\odot$.

5. SOURCES OF POSSIBLE CONTAMINATION

In this section, we discuss a surviving binary companion and light echoes as possible sources of contamination to the bolometric light curve.

5.1. *Contamination by a binary companion?*

Bloom et al. (2012) did not see any signs of a shock interaction between the SN ejecta and a companion in the early-time light curve of SN 2011fe, which places strict limits on the radius of a potential companion ($\lesssim 0.1$ R$_\odot$). However, this limit can be avoided for unfavorable viewing angles (Kasen 2010), M dwarf companions (Wheeler 2012), or rapidly rotating WD primaries (Justham 2011; Di Stefano & Kilic 2012). Using archival pre-explosion *HST* imaging, Li et al. (2011) placed significantly deeper flux limits for any source at the location of SN 2011fe than we observe in our last *HST* epoch (see Figure 1). These observations ruled out the existence of a giant companion and $\gtrsim 6.0$ M$_\odot$ main-sequence companions. Finally, using deep-spectroscopic Keck observations of SN 2011fe 963 days after $t_{B\mathrm{max}}$, Graham et al. (2015a) show that any shock-heated companion must have $T \gtrsim 10^4$ K and $L \lesssim 10^4$ L$_\odot$. Thus, if there is a companion still present, it was initially smaller than a giant and then was shock heated by the SN ejecta. However, a 1 M$_\odot$ main-sequence shock-heated companion should still be significantly fainter than the last epoch presented here (Shappee et al. 2013a; See Figure 4).

A shock-heated companion will evolve on the Kelvin-Helmholtz time of the envelope ($\sim 10^3$–10^4 years; Shappee et al. 2013a). Thus, we can approximate a potential companion as a constant source of flux because our observations span a much shorter time-scale. We find that a model including just ^{56}Ni decay and a shock-heated companion cannot adequately describe the observed light curve ($\chi^2 = 143.9$ with $\nu = 2$). If we fit the quasi-bolometric light curve including ^{56}Ni and ^{57}Co radioactive decay and a constant flux companion, we find that a constant flux source can only contribute $< 6.2 \times 10^{35}$ erg s^{-1} (~ 160 L$_\odot$) to our quasi-bolometric light curve at 90% confidence.

5.2. *Light Echoes?*

As previously mentioned, SN 2011fe is observed to have exploded into an extremely clean environment. However, the light from SN 2011fe has now decreased by more than a factor of ~ 5 million in flux, so even faint light echoes could significantly contribute to the observed light curves.

As a first step, we searched for large-scale light echoes from SN 2011fe that would not affect our photometry but would allow us to probe the interstellar medium in M101 in the vicinity of SN 2011fe. To estimate the largest angular scale a light echo from SN 2011fe could have during our last epoch we conservatively assume a scattering screen 1 kpc from SN 2011fe and use the law of cosines to find a maximum angular scale of 1.″7 in radius. We used the *F*438*W* images to search the region around SN 2011fe because dust tends to scatter blue light more efficiently than red. We subtracted all the epochs from the image acquired 1403 days after $t_{B\mathrm{max}}$ because this image had the longest total exposure time. Ten to fifteen stars in common to the images were used to transform the template image to the coordinates of the search epoch. The subtracted images were convolved with a 2-pixel Gaussian kernel to bring out low surface brightness residuals. The subtractions reveal many variable point sources in the galaxy and there is a bright artifact in the template that is likely due to a bright star off the field of view. There are also trails along the columns that are most obvious in the shorter exposures and probably due to CTE. However, there are no obvious light echoes that have changed their position over the

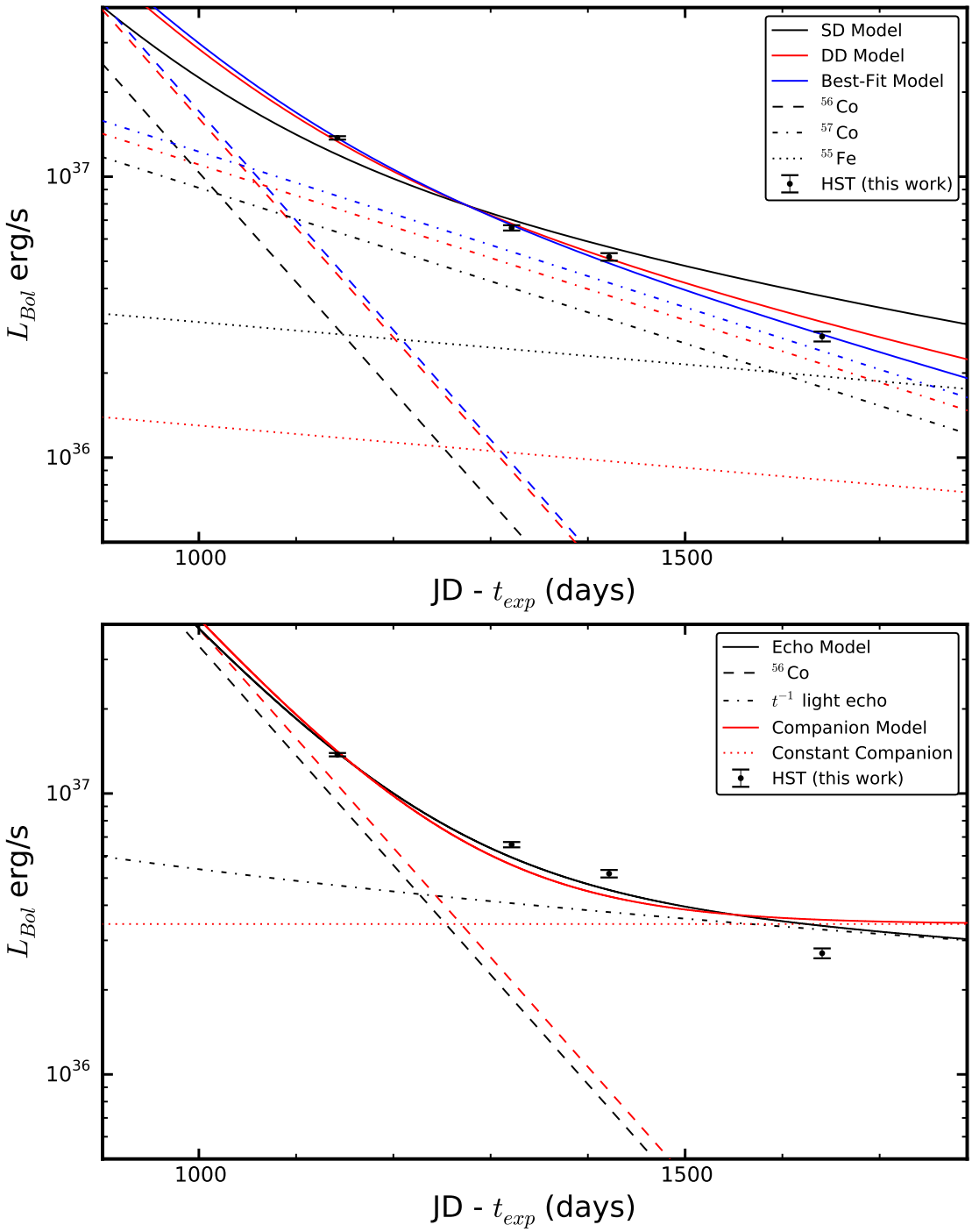

FIG. 6.— The optical+NIR quasi-bolometric light curve of SN 2011fe from 4000 – 17000 Å. **Top Panel:** The red and blue lines are the scaled SD and DD models from Röpke et al. (2012), respectively. The blue lines are the best-fit model treating ^{56}Ni, ^{57}Co/^{56}Ni and ^{55}Fe/^{57}Co as free parameters. **Bottom Panel:** The black lines are the best-fit light echo model including ^{56}Ni decay and a t^{-1} light echo. The red lines are the best-fit companion model including ^{56}Ni decay and a constant flux from a surviving SD companion.

span of a year. Using the CTE trails from the first epoch to set a conservative upper limit, we see no light echoes within a very conservative $\sim 30''$ of SN 2011fe with a surface brightness greater than 2×10^{-3} μJy square-arcsec^{-1}.

We also searched for resolved light echo in close proximity of SN 2011fe. Echoes from circumstellar material could be resolved in our last epoch with a maximum physical scale of about $2 \times c \times t \simeq 2.75$ parsecs and an angular size of $0.''089$ in diameter. In the last epoch, the nearest two sources are both 4.8 pixels ($0.''19$) away from the position of SN 2011fe. Both sources are red and are classified by DOLPHOT as point sources with magnitudes of $F438W = 30.2 \pm 1.9$, $F555W = 27.7 \pm 0.2$, and $F600LP = 26.05 \pm 0.05$ and $F555W = 27.7 \pm 0.2$ and $F600LP = 25.72 \pm 0.04$. The second source is not detected at $F438W$. Both sources are present in all of the earlier *HST* epochs, including those prior to the SN, so neither is a light echo. SN 2011fe itself is classified as a point source by DOLPHOT in every epoch. As

part of the photometric analysis, DOLPHOT produces a residual map after subtracting a model of all the detected sources. We visually inspect the residual maps around the location of SN 2011fe we see no resolved structures. Thus, there is no evidence for a resolved light echo of SN 2011fe in our data that would affect our photometry of SN 2011fe.

It is possible, however, to have an unresolved light echo along our line of sight. Unresolved light echoes are expected to fade as t^{-1} (see Graur et al. 2016). If we model the quasi-bolometric light curve including only ^{56}Co decay and an unresolved, t^{-1} light echo we obtain a poor fit ($\chi^2 = 77.2$ with $\nu = 2$; see Figure 6). Thus, our detection of ^{57}Co decay cannot be explained as a light echo. For a fit to the quasi-bolometric light curve including ^{56}Ni and ^{57}Co radioactive decay along with a t^{-1} light echo, we find that the echo can only contribute $< 8 \times 10^{35}$ erg s^{-1} (~ 210 L$_\odot$; $\sim 29\%$) to our quasi-bolometric light curve at the last epoch (1622 days after $t_{B\max}$) at 90% confidence. Perhaps the strongest evidence against an unresolved light echo, however, is the color evolution of SN 2011fe. At maximum light, SN 2011fe had $B-H = -0.85 \pm 0.04$. By 1622 days past $t_{B\max}$ SN 2011fe had $F438W - F160W = 2.3 \pm 0.1$. Light echoes are expected to be roughly the same color or bluer than the SN at peak (Patat 2005), and SN 2011fe becoming redder by a factor of ~ 20 strictly limits the flux any light echo could be contributing.

6. DISCUSSION

SN 2011fe has presented us with an exceptional opportunity to constrain SNe Ia progenitor models. A series of studies have already ruled out numerous models for the progenitor system of SN 2011fe based on interactions of the SN ejecta with a non-degenerate companion (e.g., Bloom et al. 2012; Shappee et al. 2013b) or limits on any possible companion from pre-explosion imaging (e.g., Li et al. 2011; Graham et al. 2015a). In this study, we add a novel and independent constraint. At very late times (> 1050 days after $t_{B\max}$), ^{57}Co and then ^{55}Fe become the dominate power sources for SN Ia light curves (Seitenzahl et al. 2009) and the production of these isotopes is very sensitive to the central density of the exploding white dwarf(s) (Röpke et al. 2012). Thus, very-late-time bolometric observations of SNe Ia can distinguish between the SD and DD models. Using *HST* and *LBT*, we followed the light curve of SN 2011fe for an unprecedented 1622 days past $t_{B\max}$ and over a factor of ~ 5 million in flux. We present the first clean detection of ^{57}Co powering a SN Ia light curve and estimate a mass ratio of $\log(^{57}\mathrm{Co}/^{56}\mathrm{Co}) = -1.62^{+0.08}_{-0.09}$. We do not have a clean detection of a contribution from ^{55}Fe, finding a limit of $^{55}\mathrm{Fe}/^{57}\mathrm{Co} < 0.3$ with 90% confidence. These abundance ratios strongly prefer the lower central density of DD models ($^{55}\mathrm{Fe}/^{57}\mathrm{Co} = 0.27$) over the higher central density of SD models ($^{55}\mathrm{Fe}/^{57}\mathrm{Co} = 0.68$).

Theoretically, an infrared catastrophe (IRC) was predicted for SNe Ia beyond ~ 500 days when, as a result of cooling of the eject below ~ 2000 K, emission would transition from optical/NIR [Fe II-III] lines to the mid- and far-infrared fine-structure transitions (Axelrod 1980). If an IRC occurs, it would not be possible to observe very-late-time SNe Ia light curves. Luckily, late-time observations of SNe Ia have not seen this transition (e.g., Sollerman et al. 2004; Leloudas et al. 2009; McCully et al. 2014; Kerzendorf et al. 2014; Graur et al. 2016). Fransson & Jerkstrand (2015) claim to reconcile an IRC with late-time observations of SNe Ia through the redistribution of UV emission into the optical/NIR by non-thermal scattering and fluorescence in order to make up for the reduction in thermally excited flux in the optical/NIR. However, we find that Fransson & Jerkstrand (2015) still significantly underpredicts the flux emitted in the optical/NIR by a factor of ~ 3.

Our detection makes it more likely that the flattening observed by Graur et al. (2016) in the SN 2012cg broad-band $F350LP$ light curve was also due to ^{57}Co rather than a light echo. Graur et al. (2016) estimated $\log(^{57}\mathrm{Co}/^{56}\mathrm{Co}) = -1.36^{+0.11}_{-0.13}$ for SN 2012cg, which is in mild disagreement with out estimate for SN 2011fe. However, SN 2012cg was only observed in the optical with a very broad long-pass filter. Limiting our analysis to only our optical observations of SN 2011fe, we find $\log(^{57}\mathrm{Co}/^{56}\mathrm{Co}) = -1.59^{+0.09}_{-0.11}$. This is in better agreement, but there is still a $>$ 1-sigma disagreement. It is not clear if this difference is real, due to a changing SED of SN 2012cg, the result of the metallicities of the progenitors of SN 2011fe and SN 2012cg, or caused by some other intrinsic difference between these two SNe.

Additional theoretical work is needed to determine the possible isotopic yields from a broader range of progenitor systems to address a range of remaining questions: 1) How do the masses and the mass ratios of the merging WDs affect the abundance yields? Röpke et al. (2012) only modeled the merger of a 1.1 and a 0.9 M$_\odot$ WDs, but clearly other mergers are possible. 2) Do colliding WDs produce different abundance ratios than the violent merger modeled by Röpke et al. (2012)? 3) What effect does the progenitor's metallicity have on the predicted abundances? Röpke et al. (2012) used electron fractions and initial compositions corresponding to solar metallicity for the SD and DD models, respectively, but SN 2011fe was likely sub-solar. Using the Bresolin (2007) oxygen gradient for M101, Stoll et al. (2011) determined the gas-phase metallicity at the position of SN 2011fe to be 12 + log(O/H) = 8.45 ± 0.05, or approximately 0.39 or 0.58 of Solar using the solar oxygen abundance from Delahaye & Pinsonneault (2006) or Asplund et al. (2009), respectively. Additionally, Mazzali et al. (2014) require sub-solar metallicities to model the outermost layer of the ejecta and Graham et al. (2015b) also find evidence for a subsolar metallicity through a comparative analysis of photospheric and nebular-phase spectra of SN 2011fe and SN 2011by. Clearly comprehensive theoretical studies on the effects of metallicity are warranted.

Additional observations of SN 2011fe by *HST* are also crucial. Continued observations will further constrain the ^{55}Fe to ^{57}Co abundance ratio, possibly leading to the detection of a ^{55}Fe-powered SNe Ia light curve for the first time. Additionally, as SN 2011fe fades, a shock-heated non-degenerate companion may be revealed. How long will SN 2011fe be visible? To calculate a rough lower bound, we first estimated the *HST* WFC3 UVIS limiting magnitudes for $F438W$, $F555W$, and $F600LP$ using the WFC3 UVIS Imaging exposure time calculator (ETC[9]). We assumed the Taubenberger et al. (2015) 1016-day MODS/*LBT* spectrum of SN 2011fe for the input SED, our measured location of SN 2011fe, an observing date of July 1, 2018, and 5 orbits of observations with 53 min of observing time per orbit. We found that the magnitudes corresponding to a signal-to-noise ratio of 3 for the $F438W$, $F555W$, and $F600LPW$ filters are ~ 28.9, ~ 29.1, and ~ 28.6 mag, respectively. We then made the extremely conservative

[9] http://etc.stsci.edu/etc/input/wfc3uvis/imaging/

assumption that the light curve of SN 2011fe will continue to fade at the ^{57}Co decay rate with no contribution from ^{55}Fe that would slow down the rate of decay. Under these assumptions, SN 2011fe will remain visible to *HST* WFC3 observations in $F438W$, $F555W$, and $F600LPW$ for ~ 2500, ~ 2500, and ~ 2400 days after $t_{B\mathrm{max}}$ or roughly through May 2018. This estimate ignores any effects that redistribute the bolometric flux out of the optical. Additionally, SN 2011fe will become fainter than the pre-explosion images of M101, so contamination from host-galaxy light or unrelated sources may limit how long SN 2011fe is observable. However, we again, emphasize that SNe Ia are predicted to produce 0.004 – 0.013 $M_\odot$ of ^{55}Fe, which has a half life roughly twice that of ^{57}Co and is expected to become the dominant power source ~ 1600 – 2200 days after $t_{B\mathrm{max}}$ (Röpke et al. 2012). Thus, SN 2011fe is likely to be observable for longer than our estimate. We will be obtaining three additional epochs of observations for SN 2011fe in *HST* Cycles 23, 24, and 25.

While SN 2011fe is likely to remain a uniquely well-studied event, more SN Ia with late time measurements are needed to constrain the ^{57}Co/^{56}Co ratio. These measurements are only possible for the nearest and brightest objects. While such nearby SNe Ia are rare, we are maximizing our probability to discover them with the All-Sky Automated Survey for Supernovae (ASAS-SN; Shappee et al. 2014). ASAS-SN monitors the entire visible sky in both the Northern and Southern hemispheres to find nearby SNe with a minimally biased search as possible. In the upcoming *HST* Cycle 24, time was also allocated (PI: O. Graur) to add ASASSN-14lp (Shappee et al. 2015b) and SN 2015F (Monard et al. 2015) to the sample of SNe with multi-band observations out to 900–1000 days after $t_{B\mathrm{max}}$.

The authors thank Jill Gerke, Anthony Piro, Or Graur, Armin Rest, Scott Adams, Chris Burns, Ryan Foley, and Jennifer van Saders for discussions and encouragement. We also thank Crystal Mannfolk, Susana Deustua, and the entire space telescope team for their help planning and executing these observations.

This work is supported through HST-GO-14346 and HST-GO-14166. B.S. is supported by NASA through Hubble Fellowship grant HF-51348.001 awarded by the Space Telescope Science Institute, which is operated by the Association of Universities for Research in Astronomy, Inc., for NASA, under contract NAS 5-26555. CSK and KZS are supported by NSF grants AST-1515876 and AST-1515927.

The *LBT* is an international collaboration among institutions in the United States, Italy and Germany. *LBT* Corporation partners are: The Ohio State University, and The Research Corporation, on behalf of The University of Notre Dame, University of Minnesota and University of Virginia; The University of Arizona on behalf of the Arizona university system; Istituto Nazionale di Astrofisica, Italy; *LBT* Beteiligungsgesellschaft, Germany, representing the Max-Planck Society, the Astrophysical Institute Potsdam, and Heidelberg University.

IRAF is distributed by the National Optical Astronomy Observatory, which is operated by the Association of Universities for Research in Astronomy (AURA) under a cooperative agreement with the National Science Foundation.

Funding for the SDSS and SDSS-II has been provided by the Alfred P. Sloan Foundation, the Participating Institutions, the National Science Foundation, the U.S. Department of Energy, the National Aeronautics and Space Administration, the Japanese Monbukagakusho, the Max Planck Society, and the Higher Education Funding Council for England. The SDSS Web Site is http://www.sdss.org/.

This research has made use of NASA's Astrophysics Data System Bibliographic Services.

REFERENCES

Ahn, C. P., et al. 2014, ApJS, 211, 17
Alard, C. 2000, A&AS, 144, 363
Alard, C., & Lupton, R. H. 1998, ApJ, 503, 325
Antognini, J. M., Shappee, B. J., Thompson, T. A., & Amaro-Seoane, P. 2014, MNRAS, 439, 1079
Asplund, M., Grevesse, N., Sauval, A. J., & Scott, P. 2009, ARA&A, 47, 481
Axelrod, T. S. 1980, PhD thesis, California Univ., Santa Cruz.
Bianco, F. B., et al. 2011, ApJ, 741, 20
Bloom, J. S., et al. 2012, ApJ, 744, L17
Bresolin, F. 2007, ApJ, 656, 186
Brown, P. J., Dawson, K. S., Harris, D. W., Olmstead, M., Milne, P., & Roming, P. W. A. 2012, ApJ, 749, 18
Brown, P. J., et al. 2015, ApJ, 805, 74
Cappellaro, E., Mazzali, P. A., Benetti, S., Danziger, I. J., Turatto, M., della Valle, M., & Patat, F. 1997, A&A, 328, 203
Cardelli, J. A., Clayton, G. C., & Mathis, J. S. 1989, ApJ, 345, 245
Childress, M. J., et al. 2015, ArXiv e-prints
Chomiuk, L., et al. 2012, ApJ, 750, 164
—. 2016, ApJ, 821, 119
Crotts, A. P. S. 2015, ApJ, 804, L37
Delahaye, F., & Pinsonneault, M. H. 2006, ApJ, 649, 529
Di Stefano, R., & Kilic, M. 2012, ApJ, 759, 56
Foley, R. J., & Kirshner, R. P. 2013, ApJ, 769, L1
Foreman-Mackey, D., Hogg, D. W., Lang, D., & Goodman, J. 2013, PASP, 125, 306
Fossey, S. J., Cooke, B., Pollack, G., Wilde, M., & Wright, T. 2014, Central Bureau Electronic Telegrams, 3792
Fransson, C., & Jerkstrand, A. 2015, ApJ, 814, L2
Friesen, B., et al. 2016, ArXiv e-prints
Gerke, J. R., Kochanek, C. S., Prieto, J. L., Stanek, K. Z., & Macri, L. M. 2011, ApJ, 743, 176
Gerke, J. R., Kochanek, C. S., & Stanek, K. Z. 2014, The Astronomer's Telegram, 5808
—. 2015, MNRAS, 450, 3289
Giallongo, E., et al. 2008, A&A, 482, 349
Graham, M. L., Nugent, P. E., Sullivan, M., Filippenko, A. V., Cenko, S. B., Silverman, J. M., Clubb, K. I., & Zheng, W. 2015a, MNRAS, 454, 1948
Graham, M. L., et al. 2015b, MNRAS, 446, 2073
Graur, O., Maoz, D., & Shara, M. M. 2014, MNRAS, 442, L28
Graur, O., Zurek, D., Shara, M. M., Riess, A. G., Seitenzahl, I. R., & Rest, A. 2016, ApJ, 819, 31
Horesh, A., et al. 2012, ApJ, 746, 21
Iben, Jr., I., & Tutukov, A. V. 1984, ApJS, 54, 335
Isern, J., et al. 2013, ArXiv e-prints
Johansson, J., Amanullah, R., & Goobar, A. 2013, MNRAS, L59
Justham, S. 2011, ApJ, 730, L34
Kasen, D. 2010, ApJ, 708, 1025
Kasen, D., Röpke, F. K., & Woosley, S. E. 2009, Nature, 460, 869
Katz, B., & Dong, S. 2012, arXiv:astro-ph/1211.4584
Kerzendorf, W. E., Taubenberger, S., Seitenzahl, I. R., & Ruiter, A. J. 2014, ApJ, 796, L26
Kochanek, C. S., Beacom, J. F., Kistler, M. D., Prieto, J. L., Stanek, K. Z., Thompson, T. A., & Yüksel, H. 2008, ApJ, 684, 1336
Law, N. M., et al. 2009, PASP, 121, 1395
Leloudas, G., et al. 2009, A&A, 505, 265
Leonard, D. C. 2007, ApJ, 670, 1275
Li, W., et al. 2011, Nature, 480, 348
Lundqvist, P., et al. 2015, A&A, 577, A39
Maguire, K., Taubenberger, S., Sullivan, M., & Mazzali, P. A. 2016, MNRAS, 457, 3254
Maguire, K., et al. 2013, MNRAS, 436, 222
Margutti, R., et al. 2012, ApJ, 751, 134

Matheson, T., et al. 2012, ApJ, 754, 19
Mazzali, P. A., et al. 2014, MNRAS, 439, 1959
—. 2015, MNRAS, 450, 2631
McClelland, C. M., Garnavich, P. M., Milne, P. A., Shappee, B. J., & Pogge, R. W. 2013, ApJ, 767, 119
McCully, C., et al. 2014, ApJ, 786, 134
Milne, P. A., The, L.-S., & Leising, M. D. 2001, ApJ, 559, 1019
Monard, L. A. G., et al. 2015, Central Bureau Electronic Telegrams, 4081
Munari, U., Henden, A., Belligoli, R., Castellani, F., Cherini, G., Righetti, G. L., & Vagnozzi, A. 2013, NewA, 20, 30
Nozawa, T., Maeda, K., Kozasa, T., Tanaka, M., Nomoto, K., & Umeda, H. 2011, ApJ, 736, 45
Nugent, P., Sullivan, M., Bersier, D., Howell, D. A., Thomas, R., & James, P. 2011, The Astronomer's Telegram, 3581, 1
Pakmor, R., Kromer, M., Taubenberger, S., Sim, S. A., Röpke, F. K., & Hillebrandt, W. 2012, ApJ, 747, L10
Patat, F. 2005, MNRAS, 357, 1161
Patat, F., et al. 2013, A&A, 549, A62
Pejcha, O., Antognini, J. M., Shappee, B. J., & Thompson, T. A. 2013, MNRAS, 435, 943
Pereira, R., et al. 2013, A&A, 554, A27
Richmond, M. W., & Smith, H. A. 2012, Journal of the American Association of Variable Star Observers (JAAVSO), 40, 872
Röpke, F. K., et al. 2012, ApJ, 750, L19
Schlegel, D. J., Finkbeiner, D. P., & Davis, M. 1998, ApJ, 500, 525
Seifert, W., et al. 2003, in Proc. SPIE, Vol. 4841, Instrument Design and Performance for Optical/Infrared Ground-based Telescopes, ed. M. Iye & A. F. M. Moorwood, 962–973
Seitenzahl, I. R., Taubenberger, S., & Sim, S. A. 2009, MNRAS, 400, 531
Shappee, B. J., Kochanek, C. S., & Stanek, K. Z. 2013a, ApJ, 765, 150
Shappee, B. J., & Stanek, K. Z. 2011, ApJ, 733, 124
Shappee, B. J., Stanek, K. Z., Kochanek, C. S., Gerke, J. R., & Garnavich, P. 2015a, The Astronomer's Telegram, 7392
Shappee, B. J., Stanek, K. Z., Pogge, R. W., & Garnavich, P. M. 2013b, ApJ, 762, L5
Shappee, B. J., & Thompson, T. A. 2013, ApJ, 766, 64
Shappee, B. J., et al. 2014, ApJ, 788, 48
—. 2015b, ArXiv e-prints
Smith, P. S., Williams, G. G., Smith, N., Milne, P. A., Jannuzi, B. T., & Green, E. M. 2011, ArXiv e-prints
Sollerman, J., et al. 2004, A&A, 428, 555
Stetson, P. B. 1996, PASP, 108, 851
Stoll, R., Shappee, B., & Stanek, K. Z. 2011, The Astronomer's Telegram, 3588
Stritzinger, M., Mazzali, P. A., Sollerman, J., & Benetti, S. 2006, A&A, 460, 793
Stritzinger, M., & Sollerman, J. 2007, A&A, 470, L1
Taubenberger, S., et al. 2015, MNRAS, 448, L48
Thompson, T. A. 2011, ApJ, 741, 82
Tsvetkov, D. Y., Shugarov, S. Y., Volkov, I. M., Goranskij, V. P., Pavlyuk, N. N., Katysheva, N. A., Barsukova, E. A., & Valeev, A. F. 2013, Contributions of the Astronomical Observatory Skalnate Pleso, 43, 94
Tutukov, A. V., & Yungelson, L. R. 1979, Acta Astron., 29, 665
Webbink, R. F. 1984, ApJ, 277, 355
Wheeler, J. C. 2012, ApJ, 758, 123
Williams, B. F., et al. 2014, ApJS, 215, 9
Yamaguchi, H., et al. 2015, ApJ, 801, L31
Zhang, K., et al. 2016, ApJ, 820, 67